Core–Shell Nanoparticles: Characterizing Multifunctional Materials beyond Imaging—Distinguishing and Quantifying Perfect and Broken Shells

Kristina Tschulik, Kamonwad Ngamchuea, Christoph Ziegler, Max Gregor Beier, Christine Damm, Alexander Eychmueller, and Richard G. Compton**

Core–shell nanoparticles (NPs) are amongst the most promising candidates in the development of new functional materials. Their fabrication and characterization are challenging, in particular when thin and intact shells are needed. To date no technique has been available that differentiates between *intact* and broken or cracked shells. Here a method is presented to distinguish and quantify these types of shells in a single cyclic voltammetry experiment by using the different electrochemical reactivities of the core and the shell material. A simple comparison of the charge measured during the stripping of the core material before and after the removal of the shell makes it possible to determine the quality of the shells and to estimate their thickness. As a proof-of-concept two multifunctional examples of core–shell NPs, Fe_3O_4@Au and Au@SnO_2, are used. This general and original method can be applied whenever core and shell materials show different redox properties. Because billions of NPs are probed simultaneously and at a low cost, this method is a convenient new screening tool for the development of new multifunctional core–shell materials and is hence a powerful complementary technique or even an alternative to the state-of-the-art characterization of core–shell NPs by TEM.

1. Introduction

The wish to design multifunctional materials by combining different properties, including those with diametrically different bulk behavior, has stimulated huge interest in core–shell nanoparticles (NPs) in recent years.[1–5] Amongst others, a highly promising approach is the combination of magnetic cores with noble metal shells so as to gain a NP that can be conveniently manipulated by a magnetic field while being resistive against corrosion and biocompatible or catalytically active.[6–8] Numerous examples for the beneficial use of such core–shell NPs can be found in almost any field of application—be it in modern biomedical approaches to cancer treatment (for instance in hyperthermia[9,10] or targeted drug delivery[11]), in organic synthesis,[12] plasmon-enhanced optical applications,[13] or catalysis.[14] The most commonly used core materials are iron oxide NPs typically Fe_3O_4, thanks to their excellent superparamagnetic properties, the simplicity of the synthesis and the low costs of the materials required. Noble metals such us Au,[10,15,16] Ag,[17] Pt,[18] or Pd[14] are amongst the most frequently used shell materials. The high cost for such noble metals in combination with the fact that the magnetic field/flux density provided by the core material decays with the cube of the distance from the core[19] requires for the nonmagnetic (noble metal) shell to be as thin as possible. At the same time it is vital for most applications that an *intact* shell is formed. This aspect is due to the typically significant difference in the corrosion resistance of the core and the shell, causing very effective leaching of the core material in most systems. This does not only result in the complete loss of the core functionality, but the leached out core component(s) may contaminate the system under investigation or cause erroneous results, for instance in electrocatalysis or toxicity studies.

The demand for perfect coatings may also be crucial when considering core–shell systems with a noble element as a core material, as in the case of metal/semiconductor core–shell nanoparticles. This type of state-of-the-art core–shell nanomaterials has gained major interest in recent years, for instance as nanocapacitors for energy storage and conversion.[20–22] There the difference in Fermi energies and the electrocatalytic inertness of semiconductor shells (such as SnO_2) can be used to boost the amount of electronic charge that can be stored in the metallic nanoparticle core (e.g., Au). In imperfect shells this large increase in capacitance and therefore the functionality of these attractive nanocapacitor materials is lost due to reactions

Dr. K. Tschulik, K. Ngamchuea, Prof. R. G. Compton
Department of Chemistry
Physical and Theoretical
Chemistry Laboratory
University of Oxford
South Parks Road, Oxford OX13QZ, UK
E-mail: tschulik.kristina@gmail.com;
richard.compton@chem.ox.ac.uk
Dr. C. Ziegler, M. G. Beier, Prof. A. Eychmueller
Physical Chemistry
TU Dresden, Bergstr. 66b, 01069 Dresden, Germany
C. Damm
IFW Dresden
Institute for Metallic Materials
PF 270116, D-01171 Dresden, Germany

DOI: 10.1002/adfm.201501556

© 2015 WILEY-VCH Verlag GmbH & Co. KGaA, Weinheim

of solvent molecules or dissolved species (e.g., H^+ or O_2) on the noble metal surface.[20] As the electronic charge is stored in the metal core and at the metal semiconductor interface, again a thin semiconductor shell is desired for maximum capacitance enhancement and maximum energy density. [20,23,24]

The synthesis of thin shells is inevitably a difficult task in both of the example metal/metal oxide core–shell systems due to differences in the crystal structure and lattice parameters of the core and the shell, making such systems prone to the formation of cracked or broken shells.[25] Characterizing whether the formed shells of such core–shell NPs are intact rather than broken or cracked, however, is even more challenging. To date no technique exists that allows one to directly probe whether a shell is perfect or not and to quantify the ratio of intact versus imperfectly coated core–shell NPs. Here we introduce electrochemical stripping as a technique that can provide exactly such quantification for any core–shell system that shows different electrochemical reactivities of the core and the shell in an electrolyte of choice. The analysis of Fe_3O_4@Au[26] and Au@SnO_2[26] core–shell NPs will be used as two proof-of-concept examples to demonstrate the great potential of this characterization approach.

The different electrochemical reactivity of both components in hydrochloric acid solution is employed in both cases, allowing the quantification of the ratio of intact to imperfect core–shell NPs. To achieve this, core–shell NPs are immobilized on a glassy carbon electrode (GCE) and then subjected to a single cyclic voltammetry (CV) analysis, as shown schematically in **Figure 1**. To characterize Fe_3O_4@Au NPs, the potential is first swept cathodically to reduce the Fe_3O_4 cores in partially coated core–shell NPs. As the Au shells remain intact under these conditions, perfectly coated core–shell NPs are not probed in this step. The reductive charge measured in this first reductive sweep thus quantifies the amount of Fe_3O_4 in imperfect shells. Second, the potential is swept anodically to oxidize the Au shells and thus quantify the amount of Au in NP shells. Thus, the cores embedded in intact shells are exposed. Sweeping cathodically again these cores are reduced to quantify the amount of Fe_3O_4 in originally fully coated core–shell NPs. Notably, this can be achieved in a single electrochemical measurement comprising of just two cycles. For the Au@SnO_2 an initial oxidation of imperfectly coated Au cores is followed by a reductive removal of SnO_2 shells and the subsequent oxidation of Au cores in originally intact coatings yields the same information as detailed for Fe_3O_4@Au NPs.

For a known size of cores the number of fully coated cores and the average thickness of the shell can directly be estimated from the measured charges. As such, a general, fast and simple novel technique enabling the characterization of core–shell NPs is developed. This information is gained for a statistically significant number of NPs as several billions of NPs are analyzed at the same time, which makes this a powerful new complementary technique toward the probing of few individual NPs as done by transmission electron microscopy (TEM). Importantly, and in contrast to mere microscopy or other state-of-the-art techniques, the presented technique comprises two unique features. It enables probing the quality of the core (intact or not) and also provides a means to quantify the ratio of intact to broken core–shell particles, both of which are essential information for scientists developing materials with innovative functionality combinations.

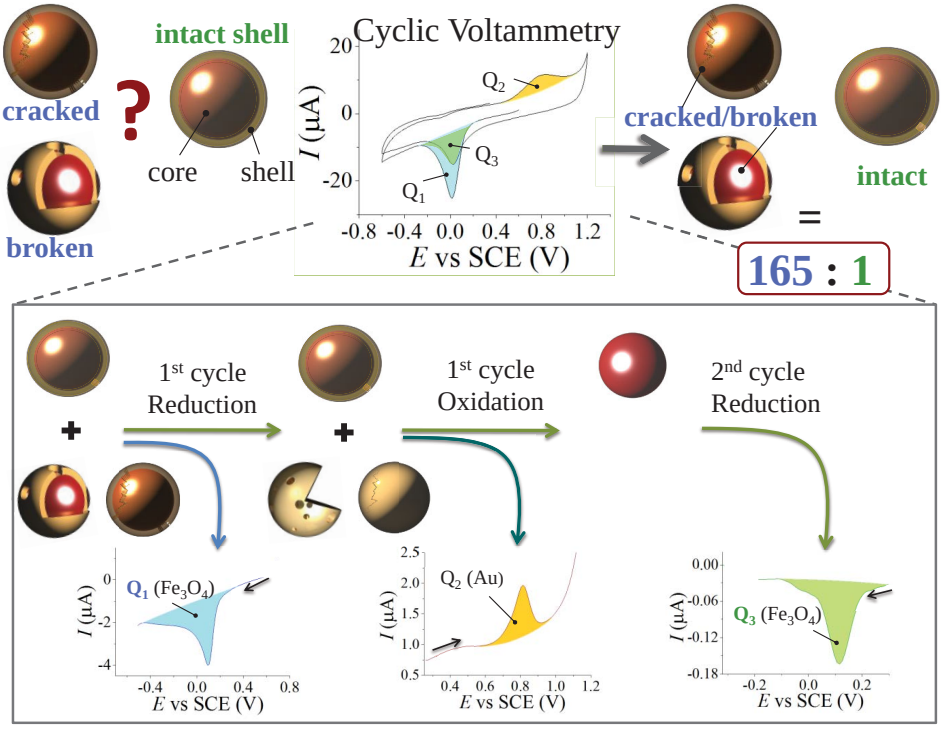

Figure 1. Schematic showing the concept of the electrochemical differentiation and quantification of intact versus cracked or broken core–shell NPs in a single CV experiment. The reductive charge Q_1 measured in the 1st cycle quantifies the amount of imperfectly coated Fe_3O_4 cores and after removal of the Au shells (oxidative charge Q_2) perfectly coated Fe_3O_4 cores are exposed and quantified by the reductive charge in the 2nd cycle (Q_3).

© 2015 WILEY-VCH Verlag GmbH & Co. KGaA, Weinheim

2. Results and Discussion

2.1. Fe_3O_4@Au Core–Shell Nanoparticles: Electrochemical Studies

The ability of the developed experimental approach to distinguish and quantify between intact and imperfect core–shell particles is first evidenced for the characterization of three different iron oxide/gold nanoparticle samples; a composite of Fe_3O_4 NPs and Au NPs (equal to fully uncoated cores), a Fe_3O_4@Au (coated cores), and a Fe_3O_4/Fe_2O_3@Au (partially oxidized coated Fe_3O_4 cores) core–shell sample. Second, the applicability to other multifunctional core–shell materials is demonstrated by using Au@SnO_2 core–shell nanoparticles as a second example.

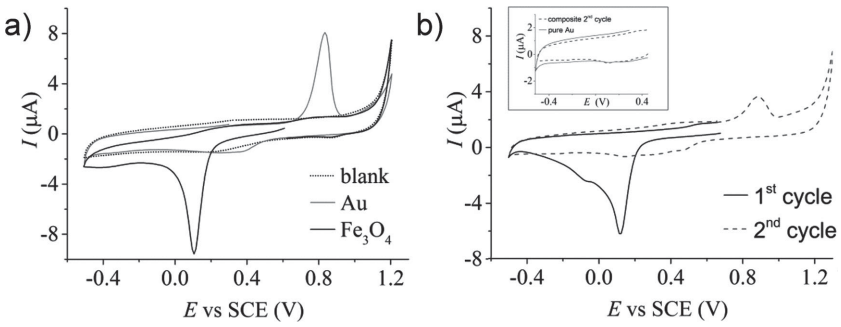

Figure 2. Cyclic voltammograms obtained using a) Au (gray) or Fe_3O_4 (black) NPs supported on a GCE and response of the unmodified GCE (dotted black line) and b) a mixture of Au and Fe_3O_4 NPs supported on a GCE, the inlay shows the 2nd reductive cycle recorded for the composite and the pure Au NPs; electrolyte: 0.1 M HCl, $dE/dt = 0.01$ V s^{-1}.

To identify suitable parameters for the electrochemical characterization of intact versus cracked or broken shells of Fe_3O_4@Au core–shell NPs, CVs were first run using the single-component NPs. Fe_3O_4 or Au NPs were supported on glassy carbon electrodes by dropcasting and then immersed in an electrolyte and subjected to CV studies (see the Experimental Section for details). As shown in **Figure 2**a, both components show clearly distinguishable electrochemical reactivities in 0.1 M HCl in the potential window of –0.5 to 1.2 V versus a saturated calomel electrode (SCE). A sweep rate of 0.01 V s^{-1} was identified to allow for quantitative stripping and clear resolution and separation of all signals. While Fe_3O_4 NPs provide a single reductive stripping peak at ≈0.1 V in the first cycle only, Au NPs show an oxidative signal at ≈0.8 V in the first and a reductive peak at about 0.4 V in the second cycle. Samples containing Fe_2O_3 show another reductive peak at about –0.25 V versus SCE (see Figure SI.1 in the Supporting Information for a CV of commercial Fe_2O_3 NPs).

These observations are in agreement with literature reports of these well-studied systems. The reduction peak observed for Fe_3O_4 has been assigned to formation of aqueous Fe^{2+}[27–29] and the oxidation and reduction peaks for Au were reported to correspond to formation and subsequent reduction of Au^{3+}.[30,31] The analysis of a mixture of Fe_3O_4 and Au NPs, that is a composite instead of a core–shell material, is shown in Figure 2b. The behavior expected from summation of the CVs of the individual particles is observed, that is Fe_3O_4 is removed in the first reductive cycle and no appearance of an additional reductive signal of Fe_3O_4 in the second cycle is seen.

Fe_3O_4@Au NPs were synthesized based on the two step route described by Williams et al.,[15] who report major difficulties in obtaining Au shells on unoxidized Fe_3O_4 cores, but only on partially oxidized Fe_3O_4/Fe_2O_3 cores, as evidenced by thorough TEM/energy dispersive X-ray spectroscopy (EDX) analysis. In a first step Fe_3O_4 cores of an average radius of 4.0 ± 1.0 nm were synthesized. In a second step these freshly prepared cores were coated with a Au shell to yield Fe_3O_4@Au NPs of a final size of about 5.1 ± 1.4 nm. Leaving the cores to partially oxidize before applying the same coating procedure yields Fe_3O_4/Fe_2O_3@Au of 6.9 ± 3.9 nm in radius. The above NP sizes were determined by TEM analysis and EDX performed after the second step confirmed the presence of Fe and Au in both core–shell products. See the Experimental Section for details on the NP synthesis and characterization.

To characterize these iron oxide/gold nanoparticle samples the respective NP suspension was dropcast onto a GCE. The NP modified electrode was then immersed into a 0.1 M HCl solution and subjected to CV stripping using the optimized parameters determined above. Starting at a potential of 0.7 V the potential was swept to –0.5 V and then to +1.2 V and back to –0.5 V at a sweep rate of 0.01 V s^{-1}. The CV obtained for Fe_3O_4@Au NPs is shown in **Figure 3**a and comprises four peaks. In the first cycle, a reduction peak (of charge Q_1) is observed at about 0.1 V and an oxidative peak is detected at ≈0.8 V (Q_2). In the second cycle two reductive signals are detected (see inlay Figure 3a), one at about 0.4 V and a second at

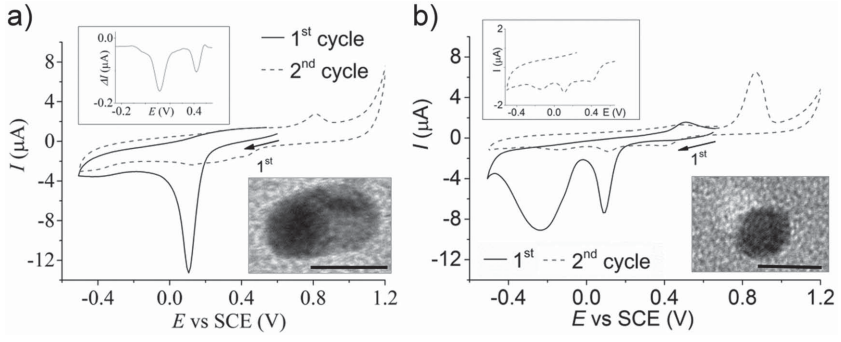

Figure 3. Cyclic voltammograms obtained at a GCE modified with a) Fe_3O_4@Au NPs, inlay: reductive signal in the second cycle after subtracting the blank plotted in Figure 2, shows two well-separated peaks according to the reduction of Au^{3+} (at 0.4 V) and the reduction of Fe_3O_4 (at 0.1 V) and b) Fe_3O_4/Fe_2O_3@Au NPs showing reductive signals of Fe_3O_4 and Fe_2O_3 in the first and the second (enlarged in inlay) reductive cycle, thus confirming the presence of intact Au shells for these partially oxidized cores; electrolyte: 0.1 M HCl, $dE/dt = 0.01$ V s^{-1}. Inlayed high-resolution TEM images of both samples indicate the presence of Au due to increased TEM contrast (scale bar = 10 nm).

© 2015 WILEY-VCH Verlag GmbH & Co. KGaA, Weinheim

Table 1. Electrochemical characterization of different core–shell samples, measured peak charges Q_1, Q_2, and Q_3 (mean of three measurements ± standard deviation), ratio of imperfect versus perfect core–shell nanoparticles in the sample, shell thickness as determined electrochemically (CV) and by TEM investigations.[36]

Sample	Q_1[a)] [μC] Imperfect core	Q_2[b)] [μC] Shell	$Q_{3(3b)}$[c)] [μC] Perfect core	Q_1:Q_3[d)] Imperfect:intact	Shell thickness [nm]	
					CV[e)]	TEM[f)]
Fe_3O_4 + Au composite	−151.3 ± 5.8	16.6 ± 0.4	No peak	>300:1	0	0
Fe_3O_4@Au	−265.0 ± 9.0	8.5 ± 0.3	−1.6 ± 0.4	≈165:1	0.1–1.2	0–2.4
Fe_3O_4/Fe_2O_3@Au	Q_1 −73.4 ± 2.6 Q_{1b} −196.0 ± 7.0	99.1 ± 2.5	Q_3 −4.8 ± 0.9 Q_{3b} −1.4 ± 0.2	≈37:1	0.5–2.9	0–6.8
Au@SnO_2	No peak	−158.5 ± 12.0	6.20 ± 0.35	<1:50	12.8–14.6	12.0–17.4
Au@SnO_2 (II)	No peak	−35.3 ± 1.4	1.82 ± 0.07	<1:50	10.7–11.6	8.8–14.6

[a)]Peak charge quantifying the cores in imperfect shells; [b)]Peak charge quantifying the shell material; [c)]Peak charge quantifying the cores in perfect shells; [d)]Ratio of cores in imperfect and intact shells; [e)]Shell thickness as determined electrochemically: lower limits represent the "cracked shell" limit (assuming that all cores probed are coated by the same amount of Au) and upper values represent the "broken shell" limit (assuming that only perfectly coated cores have a shell); [f)]Shell thickness as measured by TEM. See the Supporting Information for further details.

≈0.1 V, that is about the same position as in the first cycle (Q_3). The approach is summarized schematically in Figure 1.

Comparison of these results with CVs obtained for a GCE modified with pure Fe_3O_4 or Au NPs (Figure 2) shows that the reduction peak can be assigned to the reduction of Fe_3O_4 cores, while the oxidative charge corresponds to the oxidation of Au shells. In agreement with literature results,[27–31] Au does not contribute to the reductive signals observed at 0.1 V (Q_1) and Fe_3O_4 NPs do not show an oxidative signal under the experimental conditions used. Hence, the peaks in the first cycle can be attributed to the reduction of Fe_3O_4 NPs of imperfectly coated cores (Q_1) and the oxidation of Au in NP shells (Q_2), respectively. The cores of intact Fe_3O_4@Au NPs with an intact Au shell do *not* contribute to the first reduction peak, as the protective Au shell is not reduced under the applied conditions. Thus, these cores are reduced in the second cycle after removal of the protective Au shell in the first cycle. Consequently, the charge Q_3 (area of the peak at 0.1 V) yields the amount of Fe_3O_4 with (originally) intact Au shells.

2.2. Distinguishing Intact from Imperfect Shells

The ratio of the area of the Fe_3O_4 reduction peak in the first versus the second cycle (Q_1/Q_3) directly quantifies the amount of intact Fe_3O_4@Au NPs versus those with an imperfect shell and thus provides a very fast and convenient way not only to distinguish between fully and imperfectly coated core–shell NPs but also to quantify the ratios of both. In the experimental example the charge obtained for the first reductive cycle probing the Fe_3O_4 cores in broken or cracked shells was $Q_1 = -265.0 \pm 9.0$ μC and the charge measured during dissolving the intact Fe_3O_4 NPs was $Q_3 = -1.6 \pm 0.4$ μC. The ratio of imperfectly to fully coated core–shell NPs is 165:1 (with errors ranging from 128:1 to 228:1, as determined from three measurements). This minute number of perfectly coated Fe_3O_4 cores is consistent with the findings of Williams et al.[15] who reported that a partial oxidation of Fe_3O_4 cores to Fe_2O_3 (upon aging in the presence of oxygen) is prerequisite for a successful shell formation. Following this synthetic approach Fe_3O_4/Fe_2O_3@Au NPs core–shell particles were hence synthesized and subjected to the same cyclovoltammetric analysis as detailed above for the Fe_3O_4@Au NPs. In addition to the four previously described peaks, a fifth peak (charges Q_{1b} and Q_{3b}) corresponding to the electrochemical reduction of Fe_2O_3 to Fe^{2+} (aq) is observed in both the first and second reductive cycle, as shown in Figure 3b. See the Supporting Information for a CV of commercial Fe_2O_3 NPs.

A summary of the resulting peak charges is given in **Table 1**. As in the previous sample, again the minority of cores is perfectly coated, namely, only 1 in about 37 cores (with errors ranging from 29:1 to 45:1, as determined from three measurements).

2.3. Shell Thickness Determination

In addition to quantifying the amount of intact versus imperfect shells, the measured charges can be used to estimate the thickness of the formed shell, if the size of the cores used for the core–shell synthesis is known. For this first the charge measured for the reduction of all iron oxide cores ($Q_1 + Q_3$) is used to determine the total number of NPs analyzed. Second, the charge obtained for the Au oxidation ($Q_2 = 8.5 \pm 0.3$ μC) is used to determine the average amount of Au on each core and from that the average thickness of the shell per NP can be estimated. Assuming either one of the extreme cases that either all cores probed on average contain the same amount of Au or that only those having an intact shell are covered with Au, a lower and an upper estimate for the mean average shell thickness is obtained.

For the Fe_3O_4@Au NPs used herein, the upper estimate for the shell thickness is about 1.2 nm, while the lower estimate is below 0.10 nm. Provided that the size of a Au atom (≈0.17 nm[32] is larger than the lower estimate, it is likely that the majority of the imperfectly coated cores resemble broken core–shell NPs instead of cracked shells (where the average amount of Au per NP would be similar to that contained in an intact NP, see schematic representations of broken versus cracked shells in Figure 1). This finding of a thin/broken shell is consistent with TEM investigations (see the Experimental Section), which did not reveal a significant increase in the NP size, while EDX analysis confirmed the presence of Au and Fe_3O_4 in the sample.

Taking the charges measured for the partially oxidized Fe_3O_4/Fe_2O_3@Au core–shell NPs ($Q_2 = 99.1 \pm 2.5$ μC, see Table 1) a

© 2015 WILEY-VCH Verlag GmbH & Co. KGaA, Weinheim

much larger Au content per nanoparticle is found and the average thickness of an intact shell is estimated to about 2.9 nm. This again is in good agreement with TEM results that revealed a more pronounced increase of nanoparticle sizes after addition of the Au shell than for the previous example (see the Experimental Section). The fact that despite the increase of average particle sizes, as evidenced from microscopy, the majority of Fe_3O_4/Fe_2O_3@Au core–shell NPs has an imperfect shell, hints toward the presence of cracked rather than broken shells for this system. Thus, the lower average of the shell thickness might be more appropriate to describe the shell thickness. Thus, assuming that all cores probed have on average the same Au shell thickness a shell thickness of about 0.5 nm can be estimated. Note that considering the nonmonodispersity of cores and core–shell particles already this relatively rough estimate yields information about the average shell thickness that is about as precise as information obtainable via microscopy, yet additionally provides insight into the perfection of the formed shell.

Importantly, the number of NPs probed electrochemically is in the order of 10^8–10^{11} NPs, which provides much better statistics on the properties of a core–shell NP ensemble and makes this technique a useful complement to TEM analysis. A detailed description of the mathematical analysis is provided in the Supporting Information, TEM studies and EDX analysis are provided in the Experimental Section.

To demonstrate that this technique is not limited to core–shell systems comprising noble metal shells, but can be applied to a variety of multifunctional core–shell systems, Au@SnO_2 core–shell nanoparticles are used as a second proof-of-concept system in the following section.

2.4. Au@SnO_2 Core–Shell Nanoparticles

Two sets of Au@SnO_2 core–shell nanoparticles of 21.6 ± 1.5 nm radius (43.2 ± 3.0 nm in diameter) comprising Au cores of 6.9 ± 1.2 nm radius (13.8 ± 2.4 nm in diameter) and of 18.1 ± 1.7 nm radius (36.2 ± 3.4 nm in diameter) comprising Au cores of 6.4 ± 1.2 nm radius (12.8 ± 2.4 nm in diameter) were prepared following the two-step procedure reported by Mulvaney et al.[20] (see the Experimental Section for details). While the first batch was used as prepared, the second batch was diluted by a factor of 3 prior to the electrochemical analysis. After dropcasting 2.0 µL of either of the two nanoparticle suspensions on a GCE, cyclovoltammetric scans were run in 0.5 M HCl solution, between –1.1 and 1.2 V versus SCE at a scan rate of 0.05 V s^{-1}, to allow for quantitative stripping of SnO_2 and Au as reported elsewhere and verified in preliminary tests (not shown).[33–35]

Starting at a potential of 0.3 V versus SCE experiments comprising of two cycles were run first in either reductive (**Figure 4**a,c) or in oxidative direction (Figure 4b,d) for each of the nanoparticle samples. Both experiments show the reduction of SnO_2 shells to Sn(0) at about –0.7 V, and the oxidation of the formed Sn(0) to Sn(II) (aq)[33,34] at about –0.5 V in the first

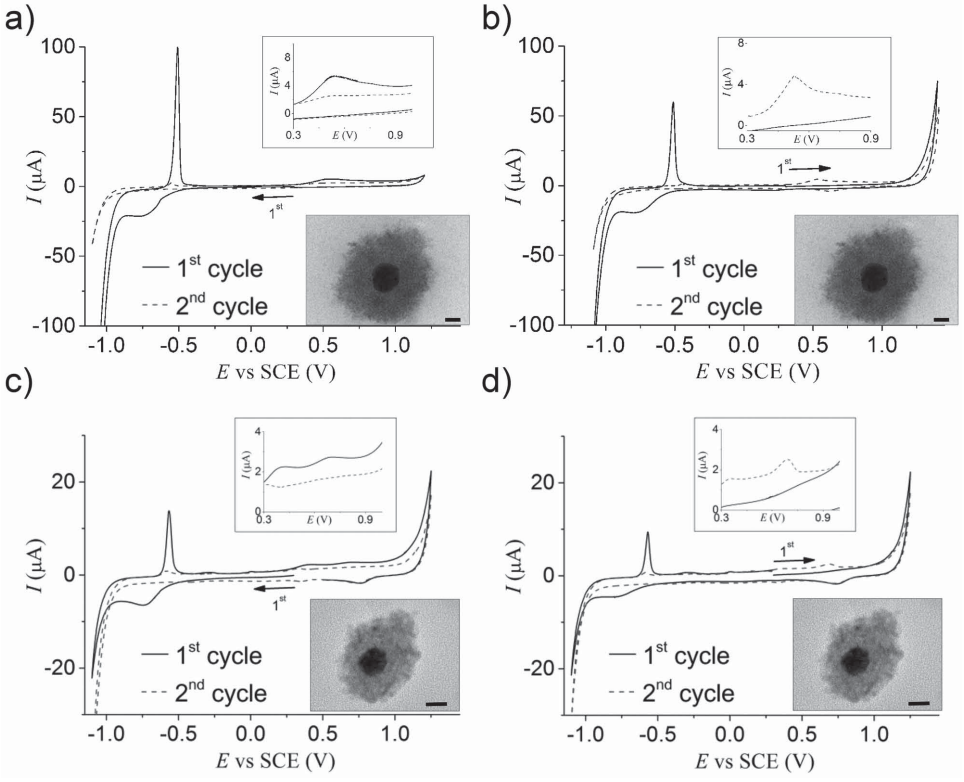

Figure 4. Cyclic voltammograms obtained at a GCE modified with two different Au@SnO_2 NP samples, when starting at 0.3 V and a,c) sweeping in cathodic direction first or b,d) initially sweeping in anodic direction; electrolyte: 0.5 M HCl, $dE/dt = 0.05$ V s^{-1}. The inlay shows that Au oxidation is only detected after reductive removal of the SnO_2 in both cases, evidencing the presence of an intact SnO_2 shell around Au cores in both samples, which is consistent with the inlayed high-resolution TEM images of both samples (scale bar = 10 nm).

© 2015 WILEY-VCH Verlag GmbH & Co. KGaA, Weinheim

cycle. The oxidation of Au cores at about 0.5 V is only detected after the reductive removal of the SnO_2 shell, that is in the 1st cycle when polarizing reductively first (Figure 4a,c) and only in the 2nd cycle when polarizing oxidatively first (Figure 4b,d). Thus, the presence of an *intact* SnO_2 shell protecting the Au cores from oxidation in both samples, Au@SnO_2 and Au@SnO_2 (II), is evidenced. Since no Au signal was observed prior to the removal of the shell in Figures 4b and d, a quantitative coating of the Au cores is verified, in agreement with Mulvaney's report.[20] Considering the experimental precision, a ratio of imperfect to intact SnO_2 shells can thus be semiquantified to not exceed 1 in 50 NPs. Note that this ratio is a conservative estimate based on the assumption that a peak more than 20 times smaller than that observed for the Au oxidation of intact cores could likely not be resolved experimentally.

Using the detected charge ratios for the reduction of SnO_2 shells ($Q_{SnO2} = -158.5 \pm 12.0$ μC) and the oxidation of "deshielded" Au cores (6.20 ± 0.35 μC) of the first Au@SnO_2 sample, the average thickness of SnO_2 shells can be estimated to about 13.7 nm (where within the stated errors it can be estimated that 14.6 nm > shell thickness > 12.8 nm, for $\approx 2 \times 10^8$ particles analyzed, see the Supporting Information). This value is in excellent agreement with the values determined by TEM analysis, which gave a shell thickness of about 14.7 ± 2.7 nm (no. of particles analyzed: 38). Analysis of the electrochemical stripping charges for the second sample Au@SnO_2 (II) yields $Q_{SnO2\_II} = -35.3 \pm 1.4$ μC for the reduction of SnO_2 shells and of $Q_{Au\_II} = 1.82 \pm 0.07$ μC for the oxidation of "deshielded" Au cores.[36] Thus, the average thickness of SnO_2 shells can be estimated to about 11.1 nm (where within the stated errors it can be estimated that 11.6 nm > shell thickness > 10.7 nm, for $\approx 9 \times 10^7$ particles analyzed). The detected thinner shell thickness of Au@SnO_2 (II) as compared to the first sample is in excellent agreement with TEM findings, as summarized in Table 1. It is noted that some TEM images showed a small number of SnO_2 nanoparticles that do not contain a Au core. The charge associated with the reduction of these particles, however, is negligible when calculating the thickness of SnO_2 shells around Au cores.[37]

2.5. Potential Applications of Electrochemical Characterization of Core–Shell Systems

The present approach is expected to find applications in two major aspects. First, it allows perfect and imperfect shells formed around any core material that can be probed/stripped electrochemically, to be differentiated and quantified. Notably this may be directly applied to any arbitrary core shape, including spheres, wires, or more complex networks and hierarchical structures. If the size of a given core particle or wire (or in case of 3D networks their surface area) is known, then the selective electrochemical stripping of the shell material can be used to determine the thickness of the shell. Existing surface sensitive electrochemical techniques, such as irreversible adsorption or under potential deposition, could potentially be used to detect imperfect shell formation in selected cases.[38,39] However, these procedures are limited to a small number of core materials (mostly noble metals), are prone to large errors due to size-dependent surface properties of nanomaterials, and do not provide information on the shell thickness.

In order to reliably quantify the ratio of perfectly versus imperfectly coated cores a suitable electrolyte system has to be chosen such that quantitative stripping of the core and the shell material occurs at different potentials. Finding a suitable electrolyte is expected not to be problematic in the majority of cases, as the typically used bi- or multifunctional core–shell nanoparticles usually comprise two components of very different chemical reactivity. However, this necessity of finding a suitable electrolyte is a drawback of he presented approach and for some core–shell systems a sequential selective stripping of the shell and the core components in different electrolytes may be required.

The electrochemical characterization of core–shell nanoparticles demonstrated herein is thought to yield valuable information of the perfection of shells that cannot currently be obtained from any other characterization technique. Due to the fact that it allows fast analysis of very large numbers of core–shell nanostructures it is also considered to provide valuable ensemble information, for instance on the average shell thickness, which can be used in combination with TEM analysis of a small number of nanoparticles, so as to allow proofing that the results of the latter technique actually provide results representative of the entire sample, rather than just a selected minority. In particular when the TEM contrast of the shell material exceeds that of the core material and when thin layers are concerned, a second independent characterization technique is required to validate TEM findings, a convenient method for this has been presented herein.

3. Conclusions

An electrochemical methodology has been developed to differentiate between core–shell NPs having a perfect shell and those with a broken or cracked shell and furthermore enables quantifying the ratio of both. As a proof-of-concept the systems Fe_3O_4@Au and Au@SnO_2 were used and it was demonstrated that this information can be obtained in a single cyclic voltammetry experiment, simply by comparison of the charge measured during the stripping of the core material before and after the removal of the shell. Moreover, the average thickness of the shell can be calculated from the stripping charge of the shell material if the size of the core is known. This is particularly valuable when thin shells are deposited, as TEM analysis may not easily allow to differentiate whether the size difference originates from an initial size distribution of the core material or the addition of a thin shell. At the same time a much larger number of NPs can be probed electrochemically than by TEM investigations, which allows one to obtain valuable and statistically relevant information on core–shell NP ensembles. Importantly, this methodology is general and can be applied to any core–shell system in which the core and the shell show different electrochemical reactivities, a condition that is an intrinsic feature of most of today's multifunctional core–shell nanoparticles. Thus, unique and valuable information on the advancing field of core–shell NPs can be gained at high throughput and low cost. In our opinion this newly developed

© 2015 WILEY-VCH Verlag GmbH & Co. KGaA, Weinheim

versatile technique may become a standard screening tool used by both laboratories developing novel core–shell systems and synthesis routes as well as by industrial producers of core–shell NPs for batch to batch quality control. Moreover, the approach can readily be applied to characterize other bi- or multifunctional nanomaterials, such as Janus[40] or supraparticles.[41]

4. Experimental Section

Fe_3O_4@Au NP Synthesis: All solutions were prepared using deionized water (Millipore) with resistivity of 18.2 MΩ cm at 25 °C. Hydrochloric acid (Sigma-Aldrich, >37%) was diluted to the concentration of 0.1 M or 0.5 M.

Fe_3O_4@Au NPs were made based on the two step method reported by Williams et al.;[15] however, in contrast to their work a citrate capping was introduced prior to the addition of the Au shell so as to avoid the partial oxidation of Fe_3O_4, which the authors suggested might generate preferential nucleation sites for the formation of the Au shell. First 10 mmol iron (II) chloride tetrahydrate ($FeCl_2{\cdot}4H_2O$, Sigma-Aldrich) and 20 mmol iron (III) chloride hexahydrate ($FeCl_3{\cdot}6H_2O$, Sigma-Aldrich) were dissolved in 27 mL solution of 0.8 M hydrochloric acid (HCl, Sigma-Aldrich). The coprecipitation of Fe_3O_4 nanoparticles (NPs) was achieved at room temperature by adding 250 mL of a 1.7 M aqueous solution of sodium hydroxide (NaOH) and stirring the reaction mixture for 30 min. Afterward, Fe_3O_4 NPs were separated from the reaction mixture with the

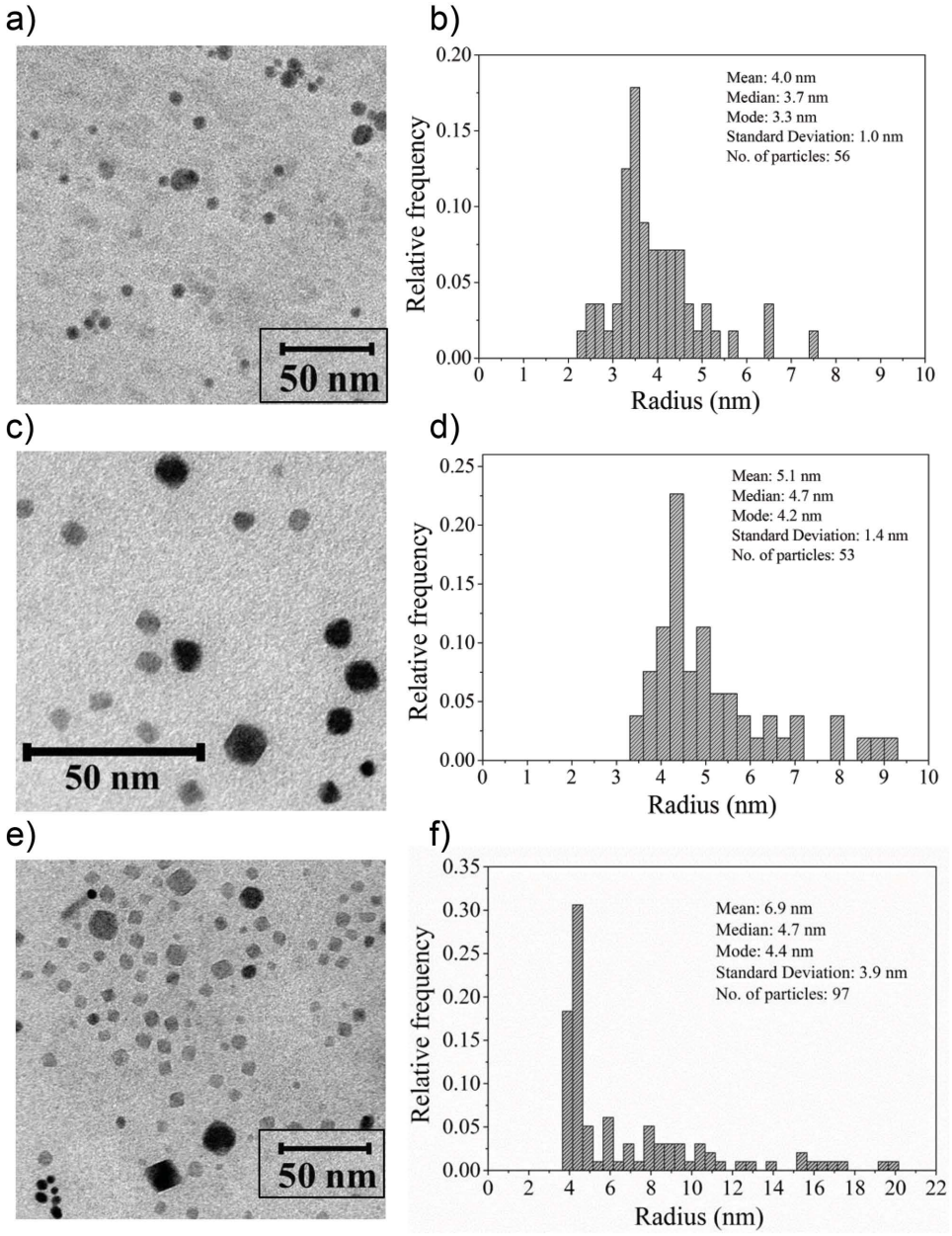

Figure 5. a) Bright-field TEM image and b) derived size distribution of the used Fe_3O_4 cores; c) bright-field TEM image, and d) derived size distribution of the used Fe_3O_4@Au nanoparticles obtained upon addition of a Au shell; e) bright-field TEM image and f) derived size distribution Fe_3O_4/Fe_2O_3@Au nanoparticles.

© 2015 WILEY-VCH Verlag GmbH & Co. KGaA, Weinheim

help of a NdFeB permanent magnet. Fe_3O_4 NPs were then washed with deionized water for three times.

Then 3.3 g of these freshly synthesized NPs were suspended in 135 mL H_2O and 3.5 g sodium citrate tribasic dihydrate was added to introduce citrate as a capping agent before the formation of the shell. This suspension was heated to 100 °C for 30 min with constant stirring and was left to cool to room temperature. The derived citrate-capped Fe_3O_4 NPs were washed with deionized water and separated from the suspension using a permanent magnet. The nanoparticles were then suspended in H_2O so as to yield a NP concentration of 3.5 g L^{-1}.

Second, the gold shell was produced at room temperature by adding 1 mmol of sodium citrate tribasic dihydrate (Sigma-Aldrich), 625 µL of 1% (w/v) gold(III) chloride solution ($HAuCl_4$, Sigma-Aldrich) and 75 µL of 0.2 M hydroxylamine hydrochloride solution ($NH_2OH{\cdot}HCl$, Sigma-Aldrich) to 10 mL of the Fe_3O_4 NP suspension. Further 400 µL $HAuCl_4$ and 400 µL $NH_2OH{\cdot}HCl$ of the same concentrations as before were added in six consecutive steps of 50 µL each for the first three times and 100 µL each for the latter three with 10 min stirring in between each addition. The solution was stirred for additional 30 min, centrifuged at 7000 rpm for 20 min and washed with deionized water for three times. After each washing the formed Fe_3O_4@Au NPs were separated from the remainder solution (and potentially formed nonmagnetic Au particles) using a NdFeB permanent magnet, so that only fully, partially or uncoated Fe_3O_4 nanoparticles remained in the NP suspension, but no pure Au NPs.

As Fe_2O_3 was reported to improve the nucleation of Au on iron oxide to yield Fe_3O_4/Fe_2O_3@Au NPs, a sample of the uncoated Fe_3O_4 NP batch was left to partially oxidize in air saturated deionized water for 36 h at 25 °C. Then the same procedure as stated for production of the freshly prepared Fe_3O_4@Au NPs was applied to give Fe_3O_4/Fe_2O_3@Au.

To characterize the CV response of the single components nanoparticles, Fe_3O_4 NPs as obtained after the citrate exchange were used and citrate capped Au NPs (provided by MINTEK, Randburg, RSA using the same reagents and laboratory equipment as stated above).

Fe_3O_4@Au NP Characterization: Fe_3O_4 nanoparticles as obtained after the citrate capping ("cores") and after the addition of the Au shell (Fe_3O_4@Au) were characterized by TEM imaging using a FEI TECNAI 20 (200 kV/LaB6-filament) and elemental analysis by energy-dispersive X-ray spectroscopy (EDX) was done in scanning TEM mode (EDX-Oxford-detector). Samples were prepared by dropcasting freshly sonicated NP stock suspension onto a carbon coated Cu or Ni TEM grid of 3 mm diameter. Au NPs were characterized via SEM imaging using a Leo Gemini II Field emission gun microscope (Zeiss, Germany).

The software package ImageJ (1.47, National Institutes of Health, USA) was used to analyze the TEM and SEM images to obtain information on the NP size distributions. Representative TEM images and histograms visualizing of the determined size distributions are shown in **Figure 5**. The average size of Fe_3O_4 cores was determined to 4.0 ± 1.0 nm in radius (diameter = 8.0 ± 2.0 nm), the radius of Fe_3O_4@Au was sized to 5.1 ± 1.4 nm (diameter = 10.2 ± 2.8 nm) and that of Fe_3O_4/Fe_2O_3@Au to 6.9 ± 3.9 nm (diameter = 13.7 ± 7.8 nm). While within experimental uncertainty a successful modification of the iron oxide cores can thus not be evidenced, elemental analysis of the core–shell nanoparticles confirmed the presences of both Au and Fe in both the core–shell samples (see **Figure 6**). Pure Au nanoparticles used as CV reference samples were sized to a mean radius of 12.9 ± 3.5 nm (diameter = 25.8 ± 7.0 nm) based on the obtained SEM images (not shown).

Au@SnO_2 Synthesis: Au@SnO_2 nanoparticles were synthesized as described by Mulvaney et al.[20] In brief, a two-step method was used to first produce Au nanoparticles, which were secondly coated with a SnO_2 shell. Au cores were prepared by heating 0.5 L of an aqueous solution of 0.4×10^{-3} M $HAuCl_4$ to boiling point. At boiling point and under rapid stirring, 25 mL of 34×10^{-3} M trisodium citrate was added. The reaction mixture was left to boil for 15 minutes and then allowed to cool to room temperature and diluted with H_2O to a Au concentration of 0.25×10^{-3} M. Thus, initially Au nanoparticles of about 6.9 ± 1.2 nm radius were formed.

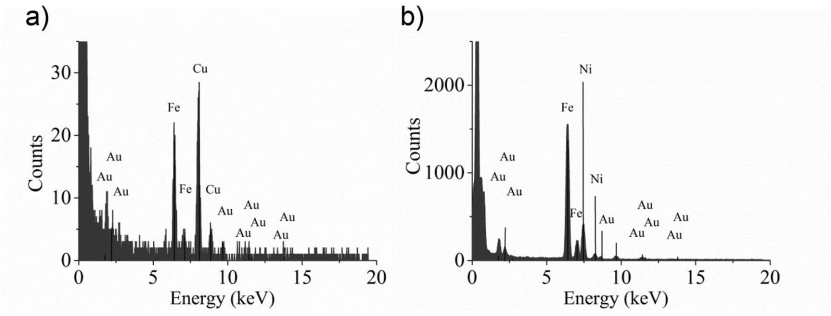

Figure 6. EDX analysis of the core–shell samples in scanning TEM mode shows the presence of both Au and Fe; a) Fe_3O_4@Au and b) Fe_3O_4/Fe_2O_3@Au. The Cu and Ni signals detected originate from the used carbon coated Cu or Ni TEM grids.

In a second step 0.1×10^{-3} M NaOH solution was added to 8 mL of this Au NP core suspension to adjust the pH of the solution to 10. A solution of 10.7 mg $Na_2Sn(OH)_6$ in 1 mL H_2O (=1.34 mg $Na_2Sn(OH)_6$ per mL Au NP core suspension) was then added to the Au core suspension and the reaction mixture was heated to 60 °C under permanent stirring. After 1 h at 60 °C the Au@SnO_2 core–shell nanoparticle suspension was left to cool to room temperature. TEM and UV–vis analysis of the product confirm the formation of core–shell nanoparticles of about 21.6 ± 1.5 nm (based on 38 particles). A second sample was prepared in a similar manner, but a reduced amount of the tin salt (= 0.89 mg $Na_2Sn(OH)_6$ per mL Au NP core suspension) was added to obtain a thinner SnO_2 shell. This second sample is referred to in this work as "Au@SnO_2 (II)." TEM and UV–vis analysis of this product confirm the formation of core–shell nanoparticles of about 18.1 ± 1.7 nm (based on 47 particles) in radius.

Au@SnO_2 Characterization: TEM imaging of the Au@SnO_2 core–shell nanoparticles and uncoated Au cores was performed in bright field mode at an acceleration voltage of 120 keV using a LIBRA TEM (Zeiss). TEM images were analyzed using ImageJ software to obtain the size distributions of the synthesized nanoparticles, as shown in **Figure** 7a–f. The Au cores were sized to 6.9 ± 1.2 nm radius (diameter = 13.8 ± 2.4 nm; based on 89 particles, mean ± standard deviation) and the Au@SnO_2 core–shell particles to 21.6 ± 1.5 nm in radius (diameter = 43.2 ± 3.0 nm; based on 38 particles) for the first nanoparticle sample. This is in very good agreement with the sizing reported by Mulvaney et al.[20]

The second sample was sized to 6.4 ± 1.2 nm radius for the Au (II) cores (diameter = 12.8 ± 2.3 nm; based on 57 particles, mean ± standard deviation) and the Au@SnO_2 (II) core–shell particles to 18.1 ± 1.7 nm in radius (diameter = 36.2 ± 3.4 nm; based on 47 particles).

While the majority of particles seen in both samples were core–shell particles, a minority of apparently uncoated Au cores and core-less SnO_2 particles was found in some images. Note that due to the low TEM contrast of the SnO_2 shell it is difficult to precisely determine the shell thickness or to identify the presence of cracks or porosity in the shell. This clearly illustrates the benefit of complementary electrochemical studies when characterizing core–shell materials.

UV–vis absorption spectra were recorded using a Cary 50 UV–vis spectrophotometer (Varian) at wavelengths of 800–300 nm and a scan rate of 300 nm min^{-1}. In agreement with literature data[20] the absorption maximum was at a wavelength of ≈520 nm for the uncoated Au cores and redshifted by ≈20 and 25 nm, respectively, upon the addition of the two different SnO_2 shell (see Figure 7g). This shift can be attributed to the change of the dielectric function of the surrounding of the Au cores introduced by the shell.[25] The increase of the UV absorbance is

© 2015 WILEY-VCH Verlag GmbH & Co. KGaA, Weinheim

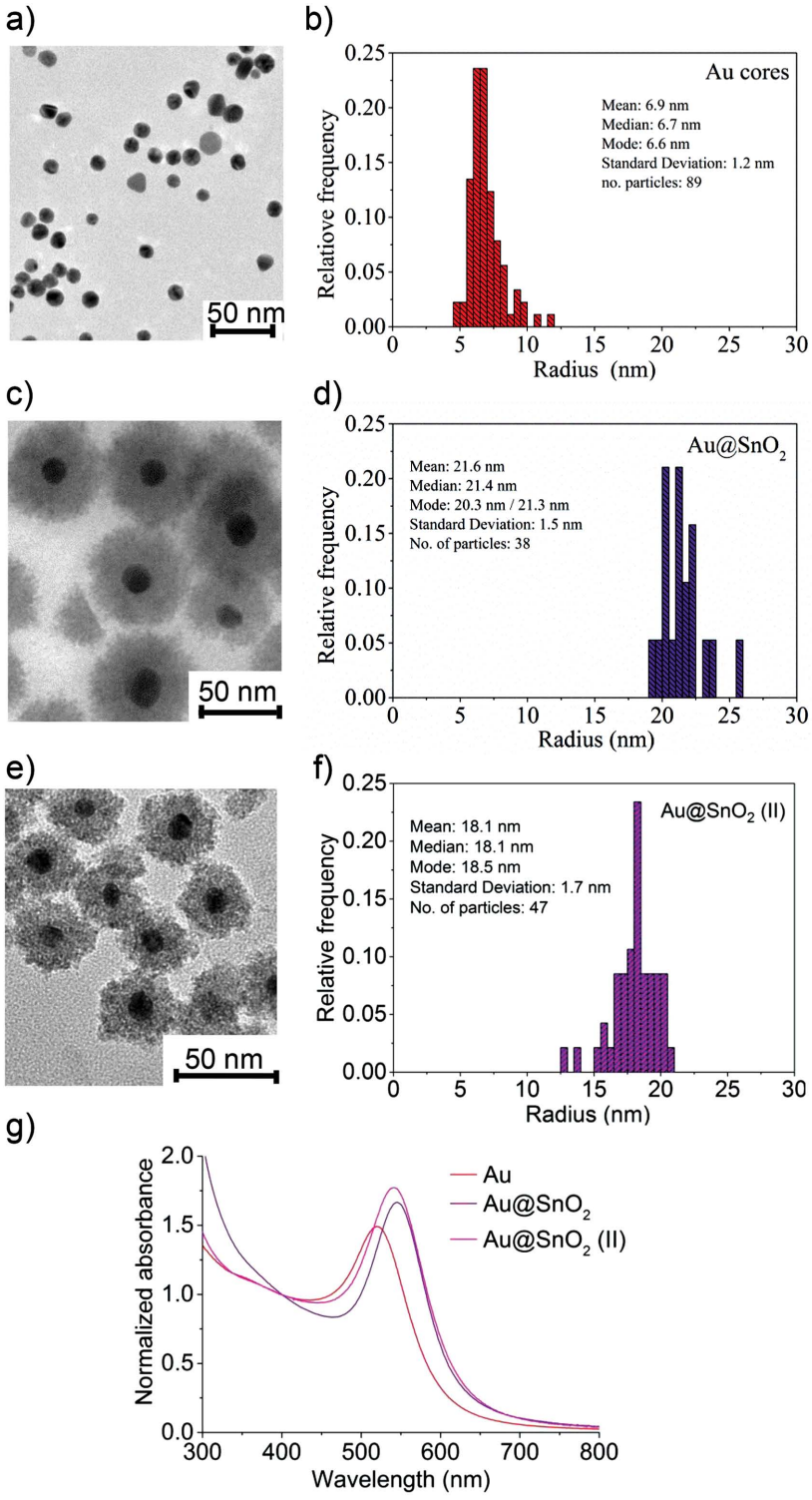

Figure 7. a) Bright-field TEM image and b) derived size distribution of the used Au cores; c,e) bright-field TEM images and d,f) derived size distributions of two different Au@SnO_2 nanoparticle samples obtained upon addition of a SnO_2 shell; g) UV–vis absorption spectra of the Au cores prior to and after the addition of SnO_2 shells of two different thicknesses, showing a redshift of the surface plasmon resonance (absorption peak) of either ≈25 nm (Au@SnO_2) or ≈20 nm (Au@SnO_2 II) upon shell addition; spectra are normalized to the absorbance at 400 nm.

due to the absorption of the SnO_2 in that spectral region.[42]

Electrochemical Characterization of Core–Shell Nanoparticles: Electrochemical experiments were performed in a thermostated (25.0 ± 0.2 °C) Faraday cage, using a μAutolab Type III potentiostat (Utrecht, Netherlands). All measurements were conducted using a standard three electrode setup utilizing a glassy carbon working electrode (GCE, BASi, USA, 3 mm diameter), a carbon rod counter electrode (3 mm diameter), and a saturated calomel reference electrode (SCE, BASi, USA).

Electrochemical Characterization of NPs Immobilized on Glassy Carbon Electrodes: For electrochemical studies known amounts of the different nanoparticles (Fe_3O_4, Fe_2O_3, Au, Fe_3O_4@Au, Fe_3O_4/Fe_2O_3@Au, and Au@SnO_2) were supported on a freshly polished glassy carbon electrode. Prior to each modification the electrode was polished using 1.0, 0.3, and 0.05 μm alumina powder (Buehler) on soft lapping pads (Buehler), then sonicated in deionized water in an ultrasonic bath for 1 minute to remove any adsorbed material. Then 2 μL of each nanoparticle suspension was dropcast onto the freshly polished surface and dried in a nitrogen flow.

For electrochemical stripping analysis of the iron oxide/gold nanoparticles CVs in deoxygenated 0.1 M HCl (aq) were recorded in the potential window between −0.5 and +1.2 V versus SCE to simultaneously analyze all surface-immobilized NPs (≈10^{11} in each case). A scan rate of 0.01 V s^{-1} was chosen for the pure NPs and the iron oxide/gold core–shell systems. To ensure quantitative removal of all exposed cores repeated cycling at reductive potentials was used if needed and the obtained charges were summed up to give the total charge quoted in the text. Studies involving Au@SnO_2 NPs were performed in 0.5 M HCl (aq) and in the potential range of −1.1 to +1.2 V versus SCE at a scan rate of 0.05 V s^{-1}. Prior to electrochemical analysis the suspension of Au@SnO_2 (II) nanoparticles was diluted with H_2O by a factor of three.

All nanoparticles studied herein were citrate capped and this ligand was found not to affect the CV response. All CV parameters were chosen such that sufficient peak separation and quantitative stripping of the nanoparticles from the electrode surface was ensured for the systems under investigation. For large nanoparticle surface coverages, repetitive reductive or oxidative cycling and summation of the peak charges (instead of running one single cyclic voltammetry scan across the entire potential range) was found to be beneficial to ensure quantitative stripping charges are gained.

The charges presented in the text and in Table 1 are mean values of three measurements and their standard deviation is used as an estimation of the experimental error (mean ± standard deviation).

Supporting Information

Supporting Information is available from the Wiley Online Library or from the author.

© 2015 WILEY-VCH Verlag GmbH & Co. KGaA, Weinheim

Acknowledgements

K.T. and K.N. contributed equally to this work. This work was supported by a Marie Curie Intra European Fellowship within the 7th European Community Framework Programme (Grant No. 327706). K.N. acknowledges funding from the Royal Thai government under the DPST Project. The authors thank H. van der Walt (MINTEK, Randburg RSA) for assistance during the NP preparation.

Received: April 17, 2015
Revised: June 12, 2015
Published online: July 14, 2015

[1] R. G. Chaudhuri, S. Paria, *Chem. Rev.* **2012**, *112*, 2373.
[2] J. Yao, M. Yang, Y. Duan, *Chem. Rev.* **2014**, *114*, 6130.
[3] M. Pumera, S. Sánchez, I. Ichinose, J. Tang, *Sens. Actuators, B* **2007**, *123*, 1195.
[4] M. Schulzendorf, C. Cavelius, P. Born, E. Murray, T. Kraus, *Langmuir* **2010**, *27*, 727.
[5] H. Matsushita, S. Mizukami, F. Sugihara, Y. Nakanishi, Y. Yoshioka, K. Kikuchi, *Angew. Chem. Int. Ed.* **2014**, *53*, 1008.
[6] V. Salgueiriño-Maceira, M. A. Correa-Duarte, *Adv. Mater.* **2007**, *19*, 4131.
[7] J. P. Liu, E. Fullerton, O. Gutfleisch, D. J. Sellmyer, *Nanoscale Magnetic Materials and Applications*, Springer Science and Business Media, Heidelberg, Germany, **2010**.
[8] M. Mahmoudi, H. Hofmann, B. Rothen-Rutishauser, A. Petri-Fink, *Chem. Rev.* **2012**, *112*, 2323.
[9] C. S. S. R. Kumar, F. Mohammad, *Adv. Drug Deliv. Rev.* **2011**, *63*, 789.
[10] M. Abdulla-Al-Mamun, Y. Kusumoto, T. Zannat, Y. Horie, H. Manaka, *RSC Adv.* **2013**, *3*, 7816.
[11] C. Sun, J. S. H. Lee, M. Zhang, *Adv. Drug Deliv. Rev.* **2008**, *60*, 1252.
[12] D. Wang, D. Astruc, *Chem. Rev.* **2014**, *114*, 6949.
[13] R. Jiang, B. Li, C. Fang, J. Wang, *Adv. Mater.* **2014**, *26*, 5274.
[14] L. Zhang, N. Zhou, B. Wang, C. Liu, G. Zhu, *J. Colloid Interface Sci.* **2014**, *421*, 1.
[15] J. L. Lyon, D. A. Fleming, M. B. Stone, P. Schiffer, M. E. Williams, *Nano Lett.* **2004**, *4*, 719.
[16] H. Zhou, J.-P. Kim, J. H. Bahng, N. A. Kotov, J. Lee, *Adv. Funct. Mater.* **2014**, *24*, 1439.
[17] P. Gong, H. Li, X. He, K. Wang, J. Hu, W. Tan, S. Zhang, X. Yang, *Nanotechnology* **2007**, *18*, 285604.
[18] M. Ma, J. Xie, Y. Zhang, Z. Chen, N. Gu, *Mater. Lett.* **2013**, *105*, 36.
[19] J. M. D. Coey, *Magnetism and Magnetic Materials*, Cambridge University Press, Cambridge, UK **2010**.
[20] G. Oldfield, T. Ung, P. Mulvaney, *Adv. Mater.* **2000**, *12*, 1519.
[21] S. Peng, L. Li, H. Tan, R. Cai, W. Shi, C. Li, S. G. Mhaisalkar, M. Srinivasan, S. Ramakrishna, Q. Yan, *Adv. Funct. Mater.* **2014**, *24*, 2155.
[22] Q. Wang, J. Xu, X. Wang, B. Liu, X. Hou, G. Yu, P. Wang, D. Chen, G. Shen, *ChemElectroChem* **2014**, *1*, 559.
[23] Z. Yu, L. Tetard, L. Zhai, J. Thomas, *Energy Environ. Sci.* **2015**, *8*, 702.
[24] C. Zhang, L. Qian, K. Zhang, S. Yuan, J. Xiao, S. Wang, *J. Mater. Chem. A* **2015**, *3*, 10519.
[25] L. M. Liz-Marzán, M. Giersig, P. Mulvaney, *Langmuir* **1996**, *12*, 4329.
[26] For convenience of the reader, the common notation of referring to core–shell NPs as "core@shell" is used herein; "Fe_3O_4@Au" denotes iron oxide cores in Au shells and "Au@SnO_2" refers to gold cores in tin oxide shells. An unambiguous alternative notation is Fe_3O_4/Au or Au/SnO_2 core–shell NPs'.
[27] W. Z. Teo, M. Pumera, *ChemPhysChem* **2014**, *15*, 3819.
[28] G. A. Kozhina, A. N. Ermakov, V. B. Fetisov, A. V. Fetisov, *Russ. J. Electrochem.* **2012**, *48*, 532.
[29] H.-J. Engell, *Z. Phys. Chem.* **1956**, *7*, 168.
[30] Y. Wang, E. Laborda, K. Tschulik, C. Damm, A. Molina, R. G. Compton, *Nanoscale* **2014**, *6*, 11024.
[31] M. Pumera, M. Aldavert, C. Mills, A. Merkoçi, S. Alegret, *Electrochim. Acta* **2005**, *50*, 3702.
[32] D. R. Lide, *CRC Handbook of Chemistry and Physics*, 89th ed., Taylor & Francis Group, Cleveland, OH, USA, **2008**.
[33] V. Pérez-Herranz, M. García-Gabaldón, J. L. Guiñón, J. García-Antón, *Anal. Chim. Acta* **2003**, *484*, 243.
[34] U. Unal, G. Somer, *Turk. J. Chem.* **2011**, *35*, 73.
[35] Y. Wang, E. Laborda, K. R. Ward, K. Tschulik, R. G. Compton, *Nanoscale* **2013**, *5*, 9699.
[36] The observed approximately five times smaller charge is due to dilution of the second sample prior to the electrochemical analysis.
[37] The consumed charge scales with the radius cubed, thus the charge according to a SnO_2 core of 7 nm radius (2.5×10^{-14} C) is much smaller than the charge of a shell of 7 nm (1.8×10^{-13} C) around a Au core of 6.9 nm radius. Even if 50% of the SnO_2 particles were core-less, the estimated shell thickness for a "real" shell charge of 1.5×10^{-13} C would only be overestimated by 0.5 nm (7 nm instead of 6.5 nm, see the Supporting Information for the equations to calculate the core and shell charges), so that this contribution of coreless shells can conveniently be neglected in most cases.
[38] M. D. Hughes, Y.-J. Xu, P. Jenkins, P. McMorn, P. Landon, D. I. Enache, A. F. Carley, G. A. Attard, G. J. Hutchings, F. King, E. H. Stitt, P. Johnston, K. Griffin, C. J. Kiely, *Nature* **2005**, *437*, 1132.
[39] J. Solla-Gullón, P. Rodríguez, E. Herrero, A. Aldaz, J. M. Feliu, *Phys. Chem. Chem. Phys.* **2008**, *10*, 1359.
[40] J. Yan, S. C. Bae, S. Granick, *Adv. Mater.* **2015**, *27*, 874.
[41] Y. Xia, T. D. Nguyen, M. Yang, B. Lee, A. Santos, P. Podsiadlo, Z. Tang, S. C. Glotzer, N. A. Kotov, *Nat. Nanotechnol.* **2011**, *6*, 580.
[42] P. Chetri, A. Choudhury, *Phys. E Low-Dimens. Syst. Nanostruct.* **2013**, *47*, 257.

© 2015 WILEY-VCH Verlag GmbH & Co. KGaA, Weinheim